Effect of Cofactor Binding and Loop Conformation on Side Chain Methyl Dynamics in Dihydrofolate Reductase†

Jason R. Schnell, H. Jane Dyson, and Peter E. Wright*

Department of Molecular Biology and Skaggs Institute for Chemical Biology, The Scripps Research Institute, 10550 North Torrey Pines Road, La Jolla, California 92037

Received August 15, 2003; Revised Manuscript Received October 29, 2003

ABSTRACT: Dihydrofolate reductase (DHFR) has several flexible active site loops that facilitate ligand binding and catalysis. Previous studies of backbone dynamics in several complexes of DHFR indicate that the time scale and amplitude of motion depend on the conformation of the active site loops. In this study, information on dynamics is extended to methyl-containing side chains. To understand the role of side chain dynamics in ligand binding and loop conformation, methyl deuterium relaxation rates of *Escherichia coli* DHFR in binary folate and ternary folate:$NADP^+$ complexes have been measured, together with χ^1 rotamer populations for threonine, isoleucine, and valine residues, determined from measurements of $^3J_{C\gamma CO}$ and $^3J_{C\gamma N}$ coupling constants. The results indicate that, in addition to backbone motional restriction in the adenosine-binding site, side chain flexibility in the active site and the surrounding active site loops is diminished upon binding $NADP^+$. Resonances for several methyls in the active site and the surrounding active site loops were severely broadened in the folate:$NADP^+$ ternary complex, suggesting the presence of motion on the chemical shift time scale. The side chains of Ile14 and Ile94, which pack against the nicotinamide and pterin rings of the cofactor and substrate, respectively, exhibit rotamer disorder in the ternary folate:$NADP^+$ complex. Conformational fluctuations of these side chains may play a role in transition state stabilization; the observed line broadening for Ile14 suggests motions on a microsecond/millisecond time scale.

Experimental and theoretical studies suggest that protein structure is frequently dynamic over a wide range of time scales. Molecular motions are implicit in several aspects of enzyme function, including ligand binding and catalysis. Thus, it is not surprising that enhanced dynamics are often observed in ligand-binding sites and active site loops. Fast motions on the picosecond/nanosecond time scale arise from simple thermal fluctuations and may play a direct role in catalytic phenomena such as electron transfer (*1*−*3*) and hydrogen tunneling (*4*, *5*). Such fast motions have also been described as a sort of lubricant for larger protein conformational changes on a physiological (microsecond/millisecond) time scale (*6*). The importance of these motions in catalysis remains controversial (*7*). However, the finding that many enzymes are most active near the edge of their stabilities, when thermal energy becomes comparable to the energy of the forces holding the enzymes together, supports the functional importance of fast motions (*8*, *9*).

Our studies have focused on the enzyme dihydrofolate reductase (DHFR)[1] from *Escherichia coli*. DHFR is responsible for maintaining the cellular pool of tetrahydrofolate (THF). DHFR produces THF by reduction of dihydrofolate (DHF) in the presence of reduced nicotinamide adenine dinucleotide phosphate (NADPH). THF is an essential coenzyme that transfers single-carbon units in the biosynthesis of purine, thymidylate, and several amino acids. The central role of THF in biosynthesis makes DHFR an attractive target for antineoplastic and antibiotic drugs, and DHFR has been the subject of numerous structural and biochemical studies. DHFR is a relatively small but structurally diverse enzyme consisting of a catalytic subdomain and an adenosine-binding subdomain. The catalytic cycle includes a number of binary and ternary complexes of substrate, cofactor, and product (*10*).

X-ray crystal structures of a series of DHFR complexes (*11*) showed that a significant portion of the catalytic subdomain consists of three flexible loops, referred to as the Met20 (residues 9−24), F-G (116−132), and G-H (142−150) loops, which surround the active site and undergo ligand-dependent conformational changes. The loops assume different conformations, termed occluded or closed or open, depending on the combination of substrate and cofactor bound. The largest conformational change occurs in the Met20 loop. In substrate complexes without cofactor, the occluded conformation is favored, in which the side chain of Met16 is inserted into the nicotinamide-binding pocket (*11*). Upon binding cofactor, Met16 is flipped out of the active site, allowing the nicotinamide ring to bind, and the

† This work was supported by Grant GM56879 from the National Institutes of Health.

* Corresponding author. E-mail: wright@scripps.edu.

[1] Abbreviations: DHFR, dihydrofolate reductase; $NADP^+$, nicotinamide adenine dinucleotide phosphate; NADPH, reduced nicotinamide adenine dinucleotide phosphate: DHNADPH, 5,6-dihydroNADPH; DHF, 7,8-dihydrofolate; THF, 5,6,7,8-tetrahydrofolate; E:folate, binary complex of DHFR with folate; E:folate:$NADP^+$, ternary complex of DHFR with folate and $NADP^+$; E:folate:DHNADPH, ternary complex of DHFR with folate and 5,6-dihydroNADPH; NMR, nuclear magnetic resonance; HSQC, heteronuclear single quantum correlation.

10.1021/bi035464z CCC: $27.50
Published on Web 12/17/2003

side chain of Met20 is packed against the nicotinamide ring and the pterin ring of the substrate. A set of hydrogen bonds between the Met20 loop and the G-H loop are broken, and a new set is formed with residues in the F-G loop, stabilizing the closed conformation. The importance of these hydrogen bonding networks has been verified by mutagenesis (*12*, *13*).

In previous work, the backbone dynamics of three DHFR complexes, which model several intermediates in the DHFR catalytic cycle, were investigated by ^{15}N spin relaxation (*14*). The binary complex with the substrate/product analogue folate (E:folate) and the ternary complex with folate and 5,6-dihydroNADPH (E:folate:DHNADPH) adopt occluded loop conformations and model the product complexes. The ternary complex with folate and oxidized cofactor (E:folate:NADP$^+$) adopts a closed loop conformation in which both the pterin ring of the substrate and the nicotinamide ring of the cofactor are in the active site, appropriately positioned for hydride transfer (*11*, *14*). The E:folate:NADP$^+$ complex thus serves as a model of the reactive Michaelis complex. The backbone dynamics of the active site loops in the occluded E:folate complex are characterized by low order parameters and nanosecond time scale motions (*14*). Upon binding NADP$^+$ to form the Michaelis complex analogue, the nanosecond time scale motions are quenched, and the order parameters are increased indicating restriction of motion. Diminished flexibility in the Met20 and F-G loops probably reflects stabilizing contacts between these two loops in the closed conformation.

Studies of side chain dynamics have the potential to reveal new and useful information, as there appears to be little correlation between backbone and side chain dynamics (*15*, *16*). In addition, attempts to correlate side chain dynamics with purely structural or chemical variables, such as solvent accessibility or local packing, have mostly failed. Motions in aliphatic side chains may be particularly informative, as they are often found at protein−ligand interfaces and within hydrophobic cores. Furthermore, the persistence of side chain motions in folded proteins could make a significant entropic contribution to protein stability.

Measurements of deuterium (^{2}H) relaxation rates can be used to determine aliphatic side chain dynamics (*17*, *18*). The advantage of measuring ^{2}H relaxation over ^{13}C relaxation is that the primary mechanism for deuterium relaxation is quadrupolar. The efficiency of the quadrupolar relaxation mechanism makes contributions from other processes such as cross-correlation with neighboring ^{1}H-^{13}C dipoles or relaxation from other nonbonded spins insignificant, thus greatly simplifying analysis (*19*). Kay and co-workers have developed a scheme in which the magnetization transfer to deuterium and subsequent relaxation delay are inserted into a conventional constant-time ^{1}H,^{13}C HSQC experiment (*17*). The deuterium relaxation is observed as the attenuation of cross-peaks in simple 2-D ^{1}H,^{13}C HSQC spectra. Thus, the problem of large deuterium line widths is avoided (as well as the need for assigning ^{2}H resonances). Methyl groups are particularly amenable to study since they often give rise to intense, well-resolved peaks. In addition, methyls are common in proteins and can, on average, increase the number of probes of motion by one-third over the measurement of backbone amide ^{15}N relaxation alone.

In the present study, side chain dynamics of the occluded E:folate and closed E:folate:NADP$^+$ complexes were studied to identify motions that correlate with cofactor binding and loop conformation. Full ^{13}C labeling and random partial deuteration of DHFR allowed measurement of $R_1(^2H)$ and $R_{1\rho}(^2H)$ relaxation rates for ∼90% of side chain methyl groups. Also, χ^1 rotamer averaging was investigated by measurement of $^3J_{C\gamma CO}$ and $^3J_{C\gamma N}$ coupling constants. The results reveal a restriction of picosecond/nanosecond motions in the active site loops and the adenosine-binding site, consistent with the changes in structure (*11*) and backbone dynamics (*14*). In addition, resonances for several methyl groups in the E:folate:NADP$^+$ ternary complex were severely broadened, indicating motion on the microsecond/millisecond chemical shift time scale.

MATERIALS AND METHODS

Sample Preparation. E. coli DHFR was overexpressed in BL21-DE3 cells (Novagen) in M9 minimal medium. Samples for measurement of deuterium relaxation rates were uniformly ^{15}N/^{13}C labeled and partially (∼45%) deuterated by cell growth on ^{15}N-ammonium sulfate and ^{13}C-glucose dissolved in 65% D_2O. Deuteration to ∼45% results in a large fraction of the isotopomer of interest ($^{13}CH_2{}^2H$). Samples for measurement of $^3J_{C\gamma N}$ and $^3J_{C\gamma CO}$ were uniformly ^{15}N/^{13}C labeled. DHFR was isolated and purified as described previously (*20*, *21*). The protein was exchanged into NMR buffer (50 mM potassium phosphate, pH 6.8, 100 mM potassium chloride, 1 mM EDTA, and 1 mM DTT in degassed, argon-saturated, and double-distilled H_2O containing 10% D_2O) to a final concentration of 2.5−3.0 mM. The E:folate complex was formed by the addition of 6-fold excess folate. The E:folate:NADP$^+$ complex was formed by the addition of 6- and 10-fold excess folate and NADP$^+$, respectively. The complexes were stored in amberized NMR tubes (Wilmad) sealed with a septum to minimize degradation of the ligands by light and/or oxidation. A binary complex of DHFR and 7,8-dihydrofolate (E:DHF) was used to resolve overlap of the methyl resonances of Met20-ϵ and Met42-ϵ in the spectrum of the E:folate complex and thereby allow measurement of deuterium relaxation data for these important residues. Since DHF is very labile and light sensitive, the E:DHF sample was prepared by addition of 6-fold excess DHF under low-light conditions in an argon-purged glovebox, freeze−pump−thawed 3 times to minimize oxidation, and flame-sealed in amberized NMR tubes.

Resonance Assignments. Methyl resonance assignments for the E:folate:NADP$^+$ complex were obtained from 3-D ^{15}N TOCSY−HSQC (*22*) and (H)C(CO)NH/H(CCO)NH spectra (*23*) on the basis of published assignments for the backbone ^{1}H,^{15}N amide resonances (*14*, *24*). Side chain methyl assignments for the E:folate complex have been published (*25*, *26*). However, deuteration results in small chemical shift changes in methyl ^{1}H and ^{13}C resonances (*27*), and assignments were therefore verified by recording the above triple-resonance experiments on the same uniformly ^{15}N/^{13}C and partially deuterated samples used for the methyl deuterium relaxation experiments. All spectra used for assignments were recorded at 28.5 °C at ^{1}H spectrometer frequencies of 500 or 750 MHz.

Stereospecific Methyl Assignments. The methyl resonances of all valine and leucine residues were stereospecifically assigned by the method of Neri and co-workers (*28*). For

this, DHFR was overexpressed on minimal media containing 10% ^{13}C-glucose (0.4 g/L) and 90% natural abundance glucose (3.6 g/L). The *pro*-R methyl was identified from the ~35 Hz ^{13}C-^{13}C splitting in a high-resolution ^{1}H,^{13}C HSQC spectrum.

^{2}H Relaxation. Methyl dynamics were probed by measurement of deuterium R_1 and $R_{1\rho}$ relaxation rates. Relaxation datasets were recorded at 28.5 °C on Bruker DRX spectrometers operating at ^{1}H frequencies of 600 and 800 MHz (92 and 123 MHz for ^{2}H) using published pulse sequences (*17*). The $R_1(I_zC_zD_z)$ experiments were recorded with delays of 0.05*, 4, 14, 20, 27, 35*, 44, 64, and 75* ms, and the $R_{1\rho}(I_zC_zD_y)$ experiments were recorded with delays of 0.25*, 2, 3.5, 5*, 7, 9, 14*, 17, and 28 ms, where I, C, and D refer to the ^{1}H, ^{13}C, and ^{2}H spins, respectively. The asterisks denote delays at which data were collected in duplicate. The contribution to relaxation from spin flips in neighboring protons ($R_1(I_zC_z)$) was measured using delays of 0.135*, 11, 30, 50, 80*, 110, 140, 170, and 210* ms and subtracted from the observed deuterium relaxation rates to obtain $R_1(^{2}H)$ and $R_{1\rho}(^{2}H)$. The deuterium relaxation rates were determined from two parameter fits to peak heights. Time points at which the peak intensity was less than 2 times the signal/noise ratio were excluded (*29*). Decay curves were fit using the program CurveFit (*30*, *31*).

Deuterium relaxation rates were fit to the Lipari−Szabo model-free parameters S^2_{axis} and τ_e, where S^2_{axis} refers to motion about the vector between the methyl carbon and the adjacent covalently bonded carbon (*17*, *32*, *33*). S^2_{axis} is derived from S^2 scaled by $[(3\cos^2\theta - 1)/2]^2$ to remove the contribution from free methyl rotation. For tetrahedral geometry, θ, the angle between the $C-C_{methyl}$ bond and the $C_{methyl}-^{2}H$ bond is 109.5°, and the S^2_{axis} is $S^2/(0.111)$. The molecular tumbling time, τ_m, was determined independently from backbone amide ^{15}N relaxation measurements. ^{15}N R_1 and R_2 relaxation data were acquired as described previously (*14*) on the same NMR samples used for the deuterium relaxation experiments. The correlation times, τ_m, were estimated from the double-trimmed mean of R_2/R_1 after removal of data from residues having significant internal motion (*34*). Absence of aggregation was verified by diffusion tensor analysis in which the anisotropies of the diffusion tensors ($\mathbf{D}_{\parallel}/\mathbf{D}_{\perp}$) were calculated from the backbone amide ^{15}N R_1 and R_2 relaxation rates. The values of $\mathbf{D}_{\parallel}/\mathbf{D}_{\perp}$ for the E:folate and E:folate:NADP$^+$ complexes were 1.14 and 1.16, respectively, consistent with previous results (*14*). The effective isotropic tumbling times were 10.54 and 9.52 ns for the E:folate and E:folate:NADP$^+$ complexes, respectively; the observed differences in the rotational correlation times probably arise from differences in protein concentration (*14*). Fitting of ^{2}H relaxation rates to S^2_{axis} and τ_e was accomplished using a modified version of ModelFree 4.0 (Arthur Palmer) substituted with the appropriate equations for deuterium quadrupolar relaxation (*35*). Isotropic tumbling was assumed: errors introduced by neglect of anisotropy are estimated to be smaller than the experimental uncertainties. The quadrupolar coupling constant (e^2qQ/h) was set to 167 kHz (*36*).

Determination of χ^1 Rotamers. $^{3}J_{C\gamma CO}$ and $^{3}J_{C\gamma N}$ coupling constants were measured using spin−echo difference spectra (*37*, *38*). Two interleaved spectra were recorded as constant-time ^{1}H,^{13}C HSQC spectra in which the 3-bond couplings were either active, or inactive, depending on positioning of the carbonyl ^{13}C ($^{3}J_{C\gamma CO}$) or amide ^{15}N ($^{3}J_{C\gamma N}$) refocusing pulse. The coupling constants were calculated from $(I_a - I_b)/I_a = 2\sin^2(\pi J_{C\gamma X} T)$), in which I_a and I_b are the signals in the absence and presence of coupling, respectively, T is the constant-time evolution period (28.6 ms), and $J_{C\gamma}X$ is the 3-bond coupling constant where X is either ^{13}CO or ^{15}N (*37*).

The coupling constants were used to calculate rotamer populations from a simple 3-site jump model (*39*, *40*) following Hennig and co-workers (*41*):

$$^{3}J_{exp}(C\gamma N) = p_{180}\,^{3}J_{trans}(C\gamma N) + (1 - p_{180})\,^{3}J_{gauche}(C\gamma N) \quad (1)$$

$$^{3}J_{exp}(C\gamma CO) = p_{-60}\,^{3}J_{trans}(C\gamma CO) + (1 - p_{-60})\,^{3}J_{gauche}(C\gamma CO) \quad (2)$$

$$p_{60} = 1 - p_{180} - p_{-60} \quad (3)$$

where p_{-60}, p_{60}, and p_{180} correspond to the populations of each rotamer, and $^{3}J_{trans}$ and $^{3}J_{gauche}$ are the coupling constants expected for full rotamer occupancy. $^{3}J_{trans}$ was set to 3.6 and 2.1 Hz for $^{3}J_{C\gamma CO}$ and $^{3}J_{C\gamma N}$, respectively, in the case of Ile and Val and 3.4 and 1.9 Hz, respectively, in the case of Thr. $^{3}J_{gauche}$ was set to 0.6 and 0.4 Hz for $^{3}J_{C\gamma CO}$ and $^{3}J_{C\gamma N}$, respectively, in the case of Ile and Val and 0.4 and 0.2 Hz, respectively, in the case of Thr (*42*).

RESULTS

^{2}H Relaxation. Methyl ^{2}H R_1 and $R_{1\rho}$ relaxation rates measured at ^{1}H spectrometer frequencies of 600 and 800 MHz are tabulated in the Supporting Information. Reliable resonance intensities could be obtained for 82 methyls in the E:folate complex and 82 methyls in the E:folate:NADP$^+$ complex. Relaxation parameters for a total of 72 methyl groups could be compared between the two complexes. Relaxation data for Val13-γ1, Met20-ϵ, Ala29-β, Met42-ϵ, Leu54-δ1, Thr68-γ2, Val75-γ1, Ala83-β, Ile94-γ2, Leu104-δ1, Thr113-γ2, and Val136-γ1 in the E:folate complex and Leu28-δ1, Val40-γ1, Val88-γ1, Val99-γ1, Leu110-δ2, and Val119-γ1 in the E:folate:NADP$^+$ complex could not be measured due to resonance overlap. In addition, peak intensities for methyl Leu24-δ1/δ2 in the E:folate complex at ^{1}H frequencies of 800 MHz were weak and could not be measured reliably. Resonances for Ala7-β, Ile14-δ1, Ala19-β, and Ala117-β in the E:folate:NADP$^+$ complex were weak at both fields, and their intensities could not be measured reliably.

Resolution of Met20/Met42 Methyl Resonances. The methyl resonances for the highly conserved residues Met20 and Met42 were overlapped in the ^{1}H,^{13}C HSQC spectrum of the E:folate complex. The side chain of Met20 plays an important role in sealing the active site in the closed loop conformation, and motions in the Met20 loop have been implicated in catalysis (*11*, *43*). Experimental mutagenesis (*44*) and quantum/classical dynamic models of DHFR kinetics (*45*) suggest that Met42 is structurally and/or dynamically coupled to Gly121 during the hydride transfer. Because of the potential importance of these residues to DHFR function, we sought to resolve their methyl resonances to measure relaxation rates. We were unable to resolve the

Table 1: Methyl Model-Free Parameters[a]

	E:folate		E:folate:NADP$^+$			E:folate		E:folate:NADP$^+$	
methyl	S^2_{axis}	τ_e	S^2_{axis}	τ_e	methyl	S^2_{axis}	τ_e	S^2_{axis}	τ_e
Met1-ϵ	0.10 (0.01)	17.0 (0.1)	0.09 (0.01)	15.5 (0.1)	Thr68-γ2[b]			0.70 (0.01)	69.2 (1.3)
Ile2-γ2	0.69 (0.02)	23.7 (1.0)	0.74 (0.03)	23.2 (2.1)	Val72-γ1	0.75 (0.04)	66.2 (3.3)	0.78 (0.12)	84.7 (11.2)
Ile2-δ1	0.42 (0.01)	17.3 (0.5)	0.48 (0.01)	16.3 (1.0)	Val72-γ2	0.74 (0.03)	53.3 (2.4)	0.78 (0.06)	73.3 (6.7)
Leu4-δ1	0.43 (0.01)	77.5 (1.3)	0.52 (0.01)	66.8 (2.1)	Thr73-γ2	0.82 (0.03)	32.4 (1.5)	0.79 (0.03)	42.9 (2.3)
Leu4-δ2	0.44 (0.03)	187.3 (6.6)	0.48 (0.05)	159.0 (10.4)	Val75-γ1[b]			0.77 (0.02)	56.3 (2.1)
Ile5-γ2	0.82 (0.07)	44.8 (3.7)	0.86 (0.11)	71.8 (9.8)	Val75-γ2	0.87 (0.03)	19.7 (1.2)	0.90 (0.04)	12.1 (1.8)
Ile5-δ1	0.68 (0.07)	24.7 (3.4)	0.80 (0.06)	25.6 (3.8)	Val78-γ1	0.80 (0.01)	35.5 (0.8)	0.85 (0.02)	28.3 (1.7)
Ala6-β	0.71 (0.05)	62.2 (3.8)	0.81 (0.09)	55.9 (6.5)	Val78-γ2	0.79 (0.02)	32.6 (0.9)	0.87 (0.02)	29.9 (1.6)
Ala7-β	0.83 (0.07)	32.8 (3.6)	*c*		Ala81-β	0.89 (0.03)	34.2 (1.3)	0.91 (0.03)	34.2 (1.6)
Leu8-δ1	0.31 (0.01)	84.4 (1.9)	0.31 (0.02)	75.9 (2.6)	Ile82-γ2	0.83 (0.01)	34.5 (0.7)	0.78 (0.03)	33.4 (1.7)
Leu8-δ2	0.24 (0.01)	54.7 (1.5)	0.28 (0.01)	41.1 (0.9)	Ile82-δ1	0.50 (0.01)	20.8 (0.8)	0.52 (0.01)	29.2 (1.5)
Ala9-β	0.79 (0.06)	15.2 (2.5)	0.77 (0.05)	27.2 (5.1)	Ala83-β[b]			0.90 (0.02)	33.4 (1.1)
Val10-γ1	0.63 (0.02)	98.0 (2.2)	0.66 (0.03)	114.4 (4.5)	Ala84-β	0.80 (0.02)	49.3 (1.3)	0.84 (0.03)	48.5 (2.2)
Val10-γ2	0.64 (0.09)	22.1 (4.3)	0.77 (0.06)	25.8 (4.9)	Val88-γ1	0.75 (0.02)	43.2 (1.0)		
Val13-γ1[b]			0.79 (0.02)	46.5 (1.9)	Val88-γ2	0.77 (0.02)	25.9 (1.0)	0.76 (0.03)	23.5 (1.6)
Val13-γ2	0.70 (0.04)	49.6 (3.0)	0.69 (0.07)	60.8 (8.7)	Ile91-γ2	0.85 (0.02)	29.6 (1.1)	0.85 (0.04)	31.9 (2.2)
Ile14-γ2	0.71 (0.03)	47.4 (1.8)	0.81 (0.10)	34.3 (7.0)	Ile91-δ1	0.76 (0.02)	13.2 (0.8)	0.80 (0.02)	19.0 (1.6)
Ile14-δ1	0.69 (0.03)	15.9 (1.4)	*c*		Met92-ϵ	0.75 (0.01)	9.4 (0.8)	0.76 (0.01)	7.6 (1.0)
Met16-ϵ	0.22 (0.01)	15.5 (0.4)	0.31 (0.01)	5.3 (0.5)	Val93-γ1	0.90 (0.03)	52.8 (1.8)	0.87 (0.03)	44.7 (2.5)
Ala19-β	0.66 (0.01)	45.5 (1.0)	*c*		Val93-γ2	0.92 (0.03)	19.5 (1.1)	0.89 (0.03)	21.9 (2.4)
Met20-ϵ[e]	0.14 (0.01)	21.6 (0.2)	0.34 (0.01)	23.5 (1.2)	Ile94-γ2[b]			0.70 (0.08)	43.9 (6.3)
Leu24-δ1[d]	0.58 (0.12)	25.9 (13.0)	0.52 (0.10)	44.8 (21.4)	Ile94-δ1	0.68 (0.05)	14.2 (2.5)	0.67 (0.05)	23.8 (3.7)
Leu24-δ2[d]	0.47 (0.06)	29.3 (4.8)	0.49 (0.16)	42.4 (13.0)	Val99-γ1	0.77 (0.03)	64.3 (2.1)		
Ala26-β	0.86 (0.04)	56.0 (2.6)	1.00 (0.01)	68.9 (0.1)	Val99-γ2	0.80 (0.02)	19.5 (1.1)	0.85 (0.05)	38.3 (4.4)
Leu28-δ1	0.36 (0.01)	46.4 (0.7)			Leu104-δ1[b]			0.47 (0.02)	46.8 (3.0)
Leu28-δ2	0.33 (0.01)	61.0 (1.5)	0.32 (0.02)	57.4 (2.3)	Leu104-δ2	0.52 (0.02)	32.9 (1.6)	0.52 (0.03)	35.3 (2.8)
Ala29-β[b]			0.91 (0.02)	37.2 (1.0)	Ala107-β	0.78 (0.03)	96.8 (3.3)	0.85 (0.05)	84.2 (4.5)
Thr35-γ2	0.75 (0.05)	21.3 (2.3)	0.78 (0.07)	21.9 (3.5)	Leu110-δ1	0.66 (0.07)	44.3 (5.3)	0.69 (0.12)	48.7 (10.4)
Leu36-δ1	0.27 (0.01)	56.7 (0.4)	0.29 (0.01)	59.4 (1.0)	Leu110-δ2	0.65 (0.04)	35.2 (3.2)		
Leu36-δ2	0.27 (0.01)	56.8 (0.4)	0.29 (0.01)	61.8 (1.2)	Leu112-δ1	0.36 (0.02)	83.2 (2.4)	0.36 (0.04)	66.6 (5.8)
Val40-γ1	0.75 (0.02)	39.6 (1.4)			Leu112-δ2	0.82 (0.06)	26.8 (3.1)	0.84 (0.06)	23.6 (4.3)
Val40-γ2	0.71 (0.03)	49.5 (2.3)	0.84 (0.05)	50.0 (4.6)	Thr113-γ2[b]			0.86 (0.04)	22.9 (3.8)
Ile41-γ2	0.80 (0.02)	30.0 (1.1)	0.79 (0.03)	29.2 (1.9)	Ile115-γ2	0.82 (0.06)	53.4 (4.8)	0.89 (0.07)	44.5 (5.3)
Ile41-δ1	0.62 (0.02)	25.4 (1.0)	0.70 (0.03)	18.1 (2.0)	Ile115-δ1	0.59 (0.04)	29.1 (2.4)	0.63 (0.05)	26.2 (4.2)
Met42-ϵ[e]	0.82 (0.01)	8.7 (0.3)	0.84 (0.02)	4.5 (0.9)	Ala117-β	0.76 (0.03)	45.7 (1.6)	*c*	
Thr46-γ2	0.61 (0.08)	30.8 (8.5)	0.58 (0.05)	47.3 (4.9)	Val119-γ1	0.27 (0.01)	76.3 (0.8)		
Ile50-γ2	0.61 (0.01)	28.7 (0.8)	0.65 (0.02)	22.7 (1.6)	Val119-γ2	0.25 (0.01)	72.6 (1.0)	0.45 (0.02)	60.8 (3.0)
Ile50-δ1	0.76 (0.03)	16.7 (1.4)	0.80 (0.04)	11.5 (2.4)	Thr123-γ2	0.50 (0.01)	51.0 (1.2)	0.69 (0.18)	30.7 (29.7)
Leu54-δ1[b]			0.71 (0.12)	64.0 (14.9)	Val136-γ1[b]			0.68 (0.02)	65.6 (1.6)
Leu54-δ2	0.81 (0.06)	40.2 (3.3)	0.82 (0.04)	43.1 (4.7)	Val136-γ2	0.67 (0.02)	62.9 (1.7)	0.68 (0.02)	58.4 (2.7)
Ile60-γ2	0.82 (0.03)	33.3 (1.2)	0.81 (0.03)	36.9 (2.5)	Ala143-β	0.92 (0.02)	41.3 (1.1)	0.87 (0.04)	40.7 (2.6)
Ile60-δ1	0.30 (0.01)	24.3 (0.5)	0.29 (0.01)	25.0 (1.1)	Ala145-β	0.82 (0.02)	46.6 (0.9)	0.78 (0.03)	46.9 (1.7)
Ile61-γ2	0.76 (0.04)	62.8 (2.8)	0.75 (0.08)	92.8 (9.4)	Ile155-γ2	0.84 (0.03)	35.8 (1.8)	0.85 (0.04)	27.8 (2.7)
Ile61-δ1	0.25 (0.01)	31.9 (1.1)	0.20 (0.01)	35.6 (2.0)	Ile155-δ1	0.73 (0.03)	6.5 (1.1)	0.77 (0.03)	13.8 (1.8)
Leu62-δ1	0.38 (0.01)	53.8 (0.8)	0.46 (0.02)	67.8 (2.9)	Leu156-δ1	0.37 (0.01)	43.4 (1.2)	0.33 (0.01)	33.2 (1.3)
Leu62-δ2	0.38 (0.01)	43.4 (1.5)	0.43 (0.04)	94.3 (6.3)	Leu156-δ2	0.37 (0.01)	54.2 (1.6)	0.32 (0.01)	39.6 (1.9)

[a] Methyl model-free parameters S^2_{axis} and τ_e extracted from fits to methyl deuterium relaxation data at ^{2}H spectrometer frequencies of 92 and 123 MHz, except where indicated. Errors are given in parentheses. [b] Relaxation data were not available due to spectral overlap of resonances. [c] Relaxation data were not available due to weak or absent resonances. [d] Relaxation data at ^{2}H spectrometer frequency of 123 MHz were not available due to weak resonance intensities. Model-free parameters were extracted from fits to relaxation data collected at a ^{2}H spectrometer frequency of 92 MHz only. [e] Parameters were extracted from relaxation data obtained on the binary complex with dihydrofolate (E:DHF; see text for details).

methyls using changes in temperature or pH. However, we were able to resolve them by substituting folate with 7,8-dihydrofolate (DHF), which is the natural substrate for DHFR. Nearly all of the methyl resonances of the DHF binary complex could be assigned by analogy with the folate binary complex; only four methyls within the substrate-binding site (Ala6-β, Ala7-β, Leu24-δ2, and Leu28-δ2) could not be assigned in this way. Methyl deuterium relaxation rates were measured at a ^{1}H spectrometer frequency of 600 MHz (92 MHz in ^{2}H). The relaxation rates were essentially unchanged from those of the E:folate complex (data not shown).

χ^1 Rotamers. Coupling constant measurements are a useful source of information on conformational averaging as well as structure (*46*) and provide insights into side chain dynamics that are complementary to those derived from relaxation measurements (*47*). The deuterium R_1 and $R_{1\rho}$ relaxation rates in CH_2D methyl groups primarily probe picosecond time scale motions, whereas rotamer transitions are more likely to occur on longer time scales (*48*, *47*). Thus, investigation of rotamer averaging provides complementary information on side chain motions. The $^3J_{C\gamma CO}$ and $^3J_{C\gamma N}$ coupling constants for isoleucine, threonine, and valine residues were measured in the E:folate and E:folate:NADP$^+$ complexes to investigate rotamer averaging. The χ^1 rotamer populations were calculated using eqs 1−3. The crystal structures 1rx7 and 1rx2 (*11*) were used for initial comparison of the extracted χ^1 angles for the E:folate and E:folate:NADP$^+$ complexes, respectively.

DISCUSSION

Methyl Dynamics. Methyl S^2_{axis} and τ_e parameters extracted from deuterium relaxation rates measured at ^{2}H frequencies of 92 and 123 MHz are summarized in Table 1. As observed for methyl groups in other proteins (*15*), the range of order parameters is large (0.09−1.00). The number of bonds

Table 2: Methyl-Type Averages for the E:Folate Complex

	average methyl S^2_{axis}	average methyl τ_e (ps)	distance to backbone (bonds)	methyls observed
Ala-β	0.80 ± 0.08	48 ± 20	1	11
Ile-γ2	0.78 ± 0.08	38 ± 12	2	11
Val-γ1/γ2	0.71 ± 0.18	48 ± 22	2	19
Thr-γ2	0.67 ± 0.14	34 ± 12	2	4
Ile-δ1	0.58 ± 0.18	20 ± 7	3	12
Leu-δ1/δ2	0.45 ± 0.17	57 ± 35	3	20
Met-ϵ	0.41 ± 0.35	14 ± 5	4	5

separating the methyl group from the peptide backbone is an important determinant of the magnitude of S^2_{axis} (Table 2). The average values of S^2_{axis} in the E:folate complex based on methyl-type are Ala-β (0.80 ± 0.08) $\approx$ Ile-γ2 (0.78 ± 0.08) > Val-γ1/γ2 (0.71 ± 0.18) $\approx$ Thr-γ2 (0.67 ± 0.14) > Ile-δ1 (0.58 ± 0.18) > Leu-δ1/δ2 (0.45 ± 0.17) $\approx$ Met-ϵ (0.41 ± 0.35). However, significant variation exists for any given methyl type, as indicated by the standard deviations of the methyl-type averages. The variation appears to increase with the number of intervening bonds from the backbone. For example, the range of S^2_{axis} values observed for Ala-β S^2_{axis} is 0.66−0.92, while the range for Met-ϵ is 0.10−0.82. The decreased variation in Ala-β order parameters is consistent with a small but significant correlation of Ala-β S^2_{axis} with backbone order parameters (*15*) since backbone amide order parameters are generally more uniform, with slightly higher values in helices and lower values in loops and termini.

The lack of correlation between backbone amide S^2 and methyl S^2_{axis} (excluding alanine) order parameters can be understood from the viewpoint of amide flexibility (*49*). There is a positive correlation between backbone amide order parameters and side chain volume. The correlation is intuitive based on the trivial example of glycine, which has the lowest average backbone S^2 value. However, the side chain volume scales with the number of rotatable bonds. Thus, longer side chains are more effective at anchoring the backbone but at the same time increase the degrees of freedom for the terminal methyl groups.

Variation of the internal correlation time, τ_e, is also large (Table 2). However, a qualitative trend is noted with the degree of substitution at the adjacent carbon. The average τ_e values for methyl types in which the adjacent carbon is tertiary (Ala-β, Ile-γ2, Leu-δ1/δ2, Thr-γ2, and Val-γ1/γ2) are about twice that of methyl groups in which the adjacent carbon is secondary (Ile-δ1 and Met-ϵ).

Methyl Dynamics in the E:Folate Complex. To account for differences in flexibility due to methyl type, the order parameters for E:folate and E:folate:$NADP^+$ are plotted as the deviation from the methyl-type averages (Figure 1). Mittermaier and co-workers (*15*) have calculated average methyl-type order parameters from a set of eight proteins. Because of the larger sample size (292 methyls vs 82 measured in the E:folate or E:folate:$NADP^+$ complex), the following average methyl-type order parameters from the study by Mittermaier et al. were used: Ala-β, 0.82; Ile-γ2, 0.71; Ile-δ1, 0.47; Leu-δ1/δ2, 0.47; Met-ϵ, 0.22; Thr-γ2, 0.72; and Val-γ1/γ2, 0.63.

Deviations of the E:folate methyl order parameters from the methyl-type averages are displayed on the X-ray structure

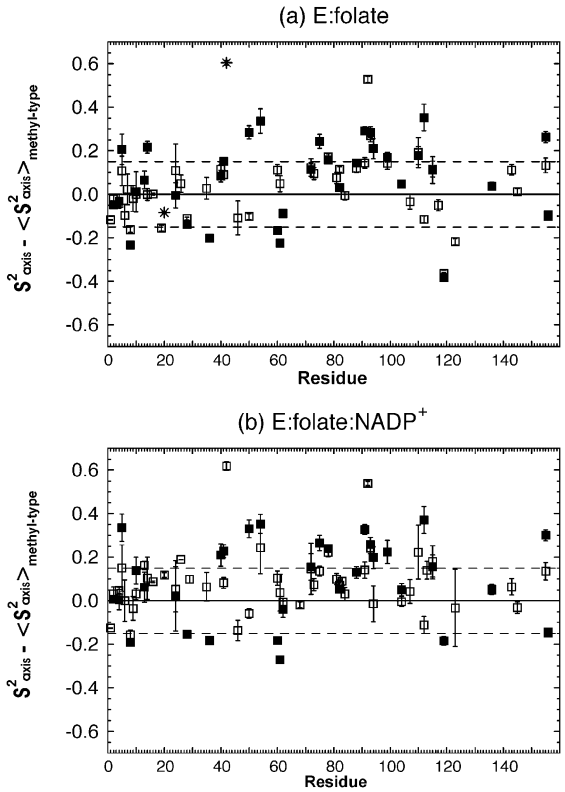

FIGURE 1: Plot of the methyl axis order parameter (S^2_{axis}) normalized by the methyl-type average as a function of the corresponding residue number for (a) E:folate and (b) E:folate:$NADP^+$. Data for methyls Ala-β, Thr-γ2, Met-ϵ, Ile-γ2, Leu-δ1, and Val-γ1 are shown as open squares, and Ile-δ1, Leu-δ2, and Val-γ2 are shown as filled squares. Methyl S^2_{axis} values are normalized by the following methyl-type averages: Ala-β, 0.81; Ile-γ2, 0.71; Ile-δ1, 0.47; Leu-δ1/δ2, 0.47; Met-ϵ, 0.22; Thr-γ2, 0.72; and Val-γ1/γ2, 0.63 (*15*). Values greater than zero indicate that motion is more restricted than expected based on methyl type. Values less than zero indicate motion that is less restricted than expected based on methyl type. Methyl order parameters were calculated from simultaneous fits to $R_1(^2H)$ and $R_{1\rho}(^2H)$ at ^1H spectrometer frequencies of 600 and 800 MHz, except where indicated. Folate binary parameters for Leu24 δ1 and δ2 are extracted from data at 600 MHz only. Folate binary values for Met20-ϵ and Met42-ϵ are derived from the dihydrofolate binary complex at (^1H) 600 MHz, which allowed separation of the corresponding resonances. Data for Met20-ϵ and Met42-ϵ are indicated with a star in panel a.

in Figure 2. Negative deviations from the average methyl-type order parameter (Figures 1 and 2) identify side chains with enhanced flexibility. The largest negative deviations occur for Val119-γ1/γ2 and Thr123-γ2 in the F-G loop. The observation of enhanced flexibility for these side chains is consistent with studies of backbone amide dynamics, which show that the F-G loop is highly flexible in the occluded state (*14*). In contrast, positive deviations from the average methyl-type order parameters, indicating more restricted motion, are observed for methyl groups of several residues within the hydrophobic core and the substrate-binding pocket. It is notable that these residues are predominantly located in the core of the adenosine-binding subdomain of DHFR; in the loop subdomain, only the δ1 methyl group of Ile14, which packs against helix F of the adenosine-binding domain, exhibits above average motional restriction (Figure 2). Methyl groups in residues throughout β-strand E (Ile91-δ1, Met92-ϵ, Val93-γ1, Val93-γ2, and Ile94-δ1) exhibit above

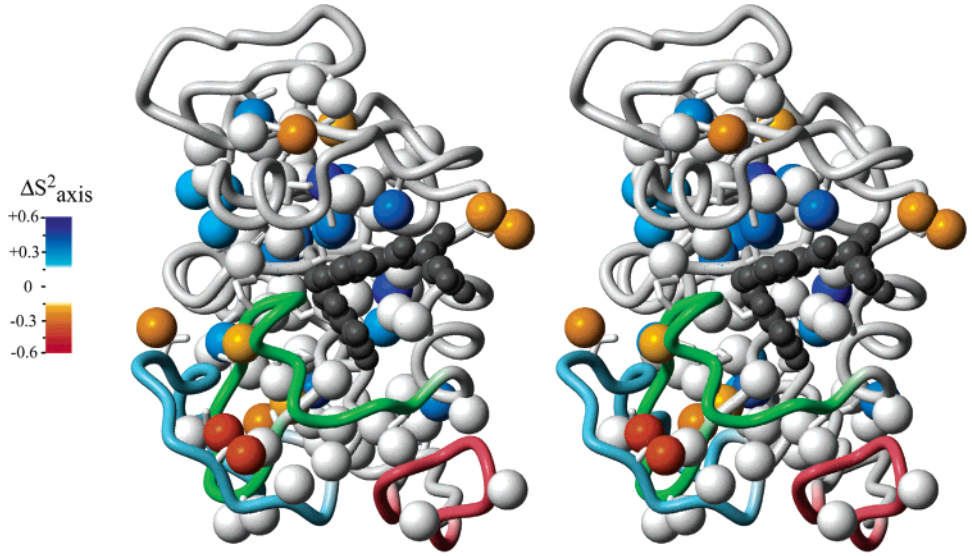

FIGURE 2: Normalized methyl S^2_{axis} values for the E:folate complex mapped onto a stereoview of the X-ray structure of the E:folate complex (1rx7) (*11*). Methyls are shown as solid spheres and color-coded to show deviations from methyl-type averages according to the scale shown. Positive deviations in S^2_{axis} indicating more restricted motion than expected based on methyl-type are shown in blue, and negative deviations indicating less restricted motion are shown in red. The backbone trace of the Met20, F-G, and G-H loop are shown in green, light blue, and red, respectively, and the atoms of the bound folate are shown as gray spheres. In the structure coordinates used to generate the figure, the χ^1 angle of Val75 was rotated to gauche− to reflect the rotamer determined from coupling constant measurements. The figure was generated using MOLMOL (*54*).

average values of S^2_{axis} (Figure 1). These residues, together with Ile50, Leu54, and Met42, form a contiguous patch of hydrophobic residues with restricted motion (Figure 2). Many of the methyl groups that form one face of the substrate-binding pocket (Ile50-δ1, Leu54-δ2, Ile94-δ1, and Ile5-δ1), or immediately abut it (Met42-ϵ and Met92-ϵ), exhibit more restricted motions. In contrast, methyl groups in side chains forming the opposite face of the substrate-binding pocket or lining the nicotinamide−ribose-binding pocket exhibit average or below average order parameters, suggesting that these regions are less tightly packed and of average or enhanced flexibility.

Methionine methyl S^2_{axis} values have been shown to have some correlation with solvent accessibility (*15*). This correlation is seen also for DHFR: the Met42-ϵ and Met92-ϵ methyls, which are buried in the hydrophobic core and are completely inaccessible to solvent, have much greater than average S^2_{axis} values. In contrast, Met1, Met16, and Met20, which have methyl order parameters close to the methyl-type average, have solvent accessible surface areas of 10−30%.

Changes in Flexibility upon Binding NADP$^+$. The differences in model-free parameters for side chain methyl groups in the ternary E:folate:NADP$^+$ complex relative to the binary E:folate complex are shown in Figure 3 and are mapped onto the structure in Figure 4. The S^2_{axis} values are generally larger in the E:folate:NADP$^+$ complex, indicating greater motional restriction of the aliphatic side chains. Some of the loss of flexibility is attributable to direct interactions with cofactor. The adenosine ring of NADP$^+$ packs against the methyls of Leu62, which exhibit slightly increased values of S^2_{axis} and τ_e in the E:folate:NADP$^+$ complex. Increases in S^2_{axis} are also observed for both methyls of Val78, which packs against the adenosine ring of NADP$^+$, and the γ2 methyl of Val99, which contacts both the adenosine ring and the pyrophosphate group. These residues form part of a hydrophobic cluster, with Phe103 at its center; interestingly, several other

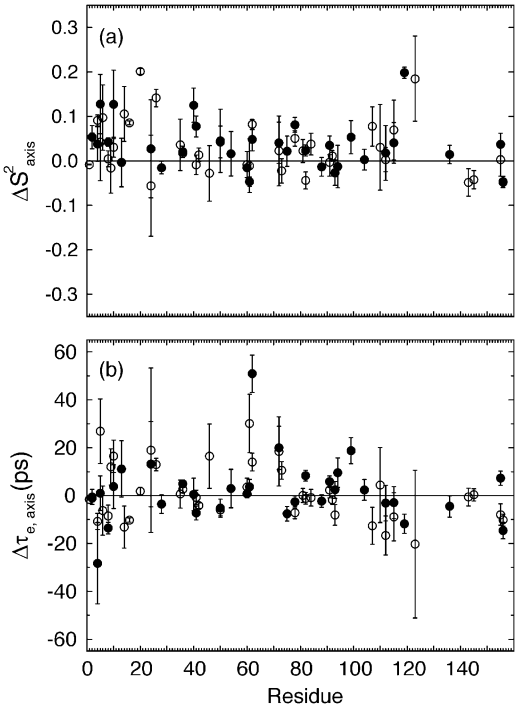

FIGURE 3: Difference in methyl (a) S^2_{axis} and (b) τ_e between the occluded E:folate and closed E:folate:NADP$^+$ complexes as a function of the corresponding residue. Differences are shown as the values for E:folate:NADP$^+$ minus those for E:folate complex. Data for methyls Ala-β, Thr-γ2, Met-ϵ, Ile-γ2, Leu-δ1, and Val-γ1 are shown as open circles, and Ile-δ1, Leu-δ2, and Val-γ2 are shown as filled circles.

methyl groups in this cluster (Ile2-γ2 and -δ2, Leu4-δ1, Ile41-δ1, and Ala107-β) also show small ($\Delta S^2 = 0.05-0.1$) increases in the order parameter, suggesting a general decrease in flexibility in the core of the adenosine-binding loop upon cofactor binding (Figure 4a). Thr123, which is partially solvent exposed in the folate binary complex, packs against the C4′ and C5′ sites of the nicotinamide-ribose

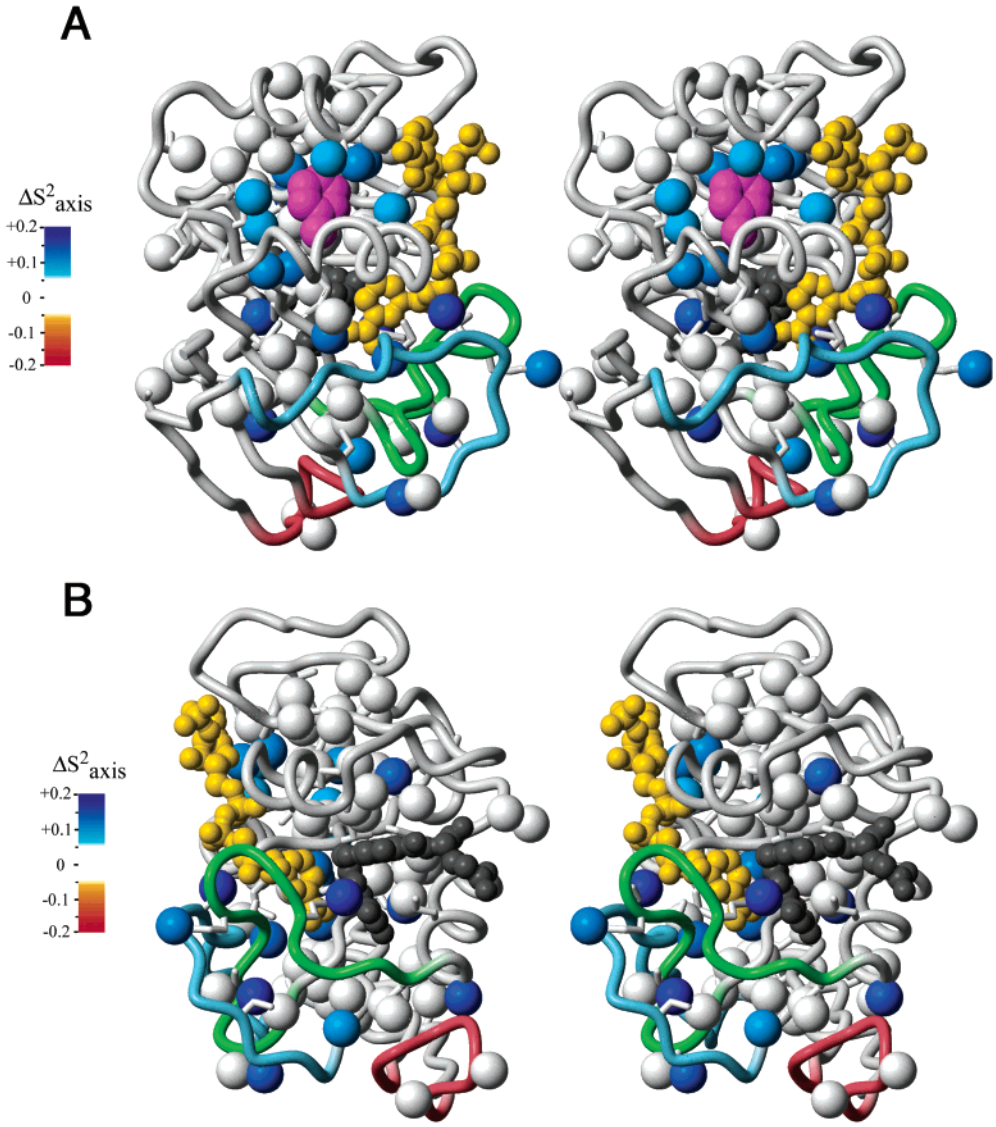

FIGURE 4: Difference in methyl S^2_{axis} mapped onto a stereoview of the E:folate:$NADP^+$ complex X-ray structure (1rx2) (*11*). (a) Back view of DHFR showing restricted motion in the adenosine-binding subdomain. (b) Front view of DHFR showing the active site and flexible loops. Methyls are shown as solid spheres and color-coded according to the scale shown. Methyls that show more restricted motion in the E:folate:$NADP^+$ complex are colored in blue. A space-filling model of the Phe103 side chain is shown in magenta in panel a. The backbone trace of the Met20, F-G, and G-H loop are shown in green, light blue, and red, respectively. In the structure coordinates used to generate the figure, the χ^1 of Val119 was rotated to gauche− to reflect the rotamer determined from coupling constant measurements. The figures were generated in MOLMOL (*54*).

moiety. The value of S^2_{axis} for Thr123-γ2 is increased by ~0.2 in the E:folate:$NADP^+$ complex.

Significant increases in methyl order parameters are also observed for several residues in the active site and the Met20 and F-G loops (Figure 4b). The E:folate:$NADP^+$ complex adopts the closed conformation, with the nicotinamide-ribose moiety of the cofactor inserted into the active site adjacent to the pterin ring of the folate (*11*, *14*). The Ala6-β and the Ile14-γ2 methyl groups, which pack against the nicotinamide ring, and the Ile5-δ1 methyl, which contacts the pterin ring of the folate, all exhibit increased S^2_{axis} values in the E:folate:$NADP^+$ complex, indicating increased motional restriction in the active site upon insertion of the nicotinamide moiety of the cofactor. Likewise, the Met20 side chain, which undergoes a large structural rearrangement on going from the occluded to the closed conformation, exhibits a large increase in S^2_{axis} upon formation of the E:folate:$NADP^+$ complex. In the closed state, the Met20-ϵ methyl packs tightly against the nicotinamide ring of the cofactor and the pterin ring of the substrate, effectively sealing off the active site and sequestering it from bulk solvent. Methyl groups in the packing interface between the Met20 and the F-G loops (Val10-γ2, Met16-ϵ, Ile115-γ2, and Val119-γ2) also become less flexible in the closed conformation (Figure 4b). These side chain motional restrictions parallel changes observed in backbone flexibility and reflect the formation of new hydrogen bonds between the Met20 and the F-G loop and tighter packing of these loops in the closed state (*14*).

χ^1 Rotamer Averaging. In the majority of isoleucine, threonine, and valine residues, a single χ^1 rotamer state predominates (>70% occupancy) in both the E:folate and the E:folate:$NADP^+$ complexes. The χ^1 rotamer populations are summarized in Table 3, together with the χ^1 dihedral angles in the X-ray structures (1rx7 and 1rx2, respectively). The agreement with the X-ray structures is good for residues where coupling constant data indicate a single predominant

Table 3: χ^1 Rotamer Populations Calculated from $^3J_{C\gamma CO}$ and $^3J_{C\gamma N}$[a]

	E:folate				E:folate:NADP$^+$			
	p_{-60}	p_{60}	p_{180}	X-ray[b]	p_{-60}	p_{60}	p_{180}	X-ray[b]
Ile2	0.92 (0.06)	0.08 (0.04)	0.00 (0.09)	−74	0.91 (0.06)	0.09 (0.04)	0.00 (0.10)	−69
Ile5	0.32 (0.15)	0.05 (0.08)	0.63 (0.23)	170	0.00 (0.24)	0.00 (0.13)	1.00 (0.36)	172
Ile14	0.52 (0.06)	0.48 (0.04)	0.00 (0.10)	46	0.01 (0.20)	0.68 (0.03)	0.31 (0.24)	57
Ile41	0.90 (0.06)	0.10 (0.03)	0.00 (0.09)	−60	0.89 (0.07)	0.03 (0.04)	0.08 (0.10)	−70
Ile50	0.88 (0.06)	0.12 (0.04)	0.00 (0.10)	−88	0.93 (0.06)	0.06 (0.04)	0.01 (0.09)	−68
Ile60	0.94 (0.07)	0.02 (0.05)	0.04 (0.11)	−59	0.94 (0.06)	0.06 (0.04)	0.00 (0.10)	−68
Ile61	0.85 (0.09)	0.01 (0.07)	0.14 (0.12)	−60	0.80 (0.11)	0.00 (0.09)	0.20 (0.15)	−38
Ile82	0.87 (0.05)	0.13 (0.03)	0.00 (0.10)	−62	0.99 (0.06)	0.01 (0.04)	0.00 (0.10)	−69
Ile91	0.91 (0.05)	0.09 (0.04)	0.00 (0.09)	−62	0.94 (0.06)	0.06 (0.03)	0.00 (0.09)	−69
Ile94[c]	0.39 (0.08)	0.48 (0.04)	0.13 (0.11)	61	0.02 (0.19)	0.52 (0.03)	0.46 (0.22)	71
Ile115	0.89 (0.11)	0.00 (0.09)	0.11 (0.16)	−61	0.62 (0.11)	0.00 (0.09)	0.38 (0.16)	−50
Ile155	0.70 (0.09)	0.00 (0.07)	0.30 (0.13)	−65	0.88 (0.06)	0.05 (0.03)	0.07 (0.09)	−60
Thr35	0.00 (0.18)	0.53 (0.03)	0.47 (0.21)	71	0.44 (0.13)	0.56 (0.03)	0.00 (0.16)	69
Thr46	0.92 (0.07)	0.08 (0.05)	0.00 (0.12)	−55	0.90 (0.11)	0.05 (0.10)	0.05 (0.16)	−64
Thr68				52	0.25 (0.06)	0.63 (0.04)	0.12 (0.10)	−71
Thr73	0.88 (0.06)	0.12 (0.04)	0.00 (0.10)	−43	0.94 (0.07)	0.06 (0.04)	0.00 (0.10)	−60
Thr113				−41	0.66 (0.08)	0.34 (0.04)	0.00 (0.11)	−62
Thr123	0.64 (0.05)	0.07 (0.03)	0.29 (0.10)	78	0.85 (0.14)	0.15 (0.07)	0.00 (0.21)	−53
Val10	0.15 (0.03)	0.11 (0.09)	0.74 (0.06)	−170	0.00 (0.04)	0.33 (0.09)	0.67 (0.06)	171
Val13[c]	0.13 (0.03)	0.00 (0.09)	0.87 (0.06)	171	0.64 (0.03)	0.00 (0.09)	0.36 (0.06)	172
Val40	0.91 (0.03)	0.04 (0.18)	0.05 (0.15)	−64				−61
Val72	0.71 (0.03)	0.12 (0.17)	0.17 (0.15)	−60	0.94 (0.05)	0.06 (0.30)	0.00 (0.26)	−59
Val75[c]	0.81 (0.03)	0.09 (0.12)	0.10 (0.08)	128	0.90 (0.03)	0.10 (0.15)	0.00 (0.12)	−63
Val78	0.25 (0.03)	0.00 (0.09)	0.75 (0.06)	−167	0.27 (0.04)	0.00 (0.10)	0.73 (0.06)	161
Val88[c]	0.72 (0.03)	0.21 (0.09)	0.07 (0.06)	−58	0.62 (0.03)	0.28 (0.09)	0.10 (0.06)	−63
Val93	0.15 (0.04)	0.10 (0.10)	0.75 (0.07)	168	0.06 (0.05)	0.16 (0.10)	0.78 (0.07)	165
Val99	0.29 (0.03)	0.00 (0.10)	0.71 (0.06)	180				173
Val119[c]	0.46 (0.03)	0.19 (0.09)	0.35 (0.06)	−28	0.68 (0.03)	0.18 (0.10)	0.14 (0.07)	117
Val136	0.63 (0.03)	0.30 (0.10)	0.07 (0.06)	−68	0.78 (0.03)	0.08 (0.10)	0.14 (0.06)	−54

[a] Rotamer populations were calculated using eqs 1−3 in Materials and Methods. [b] Values of χ^1 observed in the representative X-ray structures 1rx7 and 1rx2 for the E:folate and E:folate:NADP$^+$ complexes, respectively (*11*). [c] Some methyl resonances that could not be resolved in the deuterium relaxation experiments could be resolved in the χ^1 coupling constants experiments: Val13-γ2, Val75-γ1, and Ile94-γ2 in the E:folate complex and Val88-γ1 and Val119-γ1 in the E:folate:NADP$^+$ complex.

χ^1 rotamer. Discrepancies, however, were noted for Val75 in the E:folate complex: χ^1 in the X-ray structure 1rx7 is +128°, whereas the coupling constant data show that the $\chi^1 = -60°$ rotamer is strongly preferred (81% population). However, three additional crystal structures of the E:folate complex in different space groups are available in the Protein Data Bank (PDB) (1dyi, 1rd7, and 1re7) (*11*, *50*). In contrast to 1rx7, the χ^1 values for Val75 in these crystal structures range from −46 to −57°, in agreement with the coupling constant data. It is interesting to note that in the $\chi^1 = -60°$ rotamer, the Val75 γ2 methyl group is buried in the protein core, consistent with its above average S^2, whereas it is solvent exposed in the 1rx7 crystal structure. Coupling constant data for Val119 in the E:folate:NADP$^+$ complex indicate a significant population (68%) of the $\chi^1 = -60°$ rotamer; however, in the X-ray structure 1rx2, Val119 has an intermediate χ^1 angle of 117°. Additional structures of the E:folate:NADP$^+$ complex crystallized in different space groups are also present in the PDB (1ra2, 1rb2, and 7dfr): values of χ^1 in these structures range from −45 to −48°, consistent with the experimentally determined coupling constants.

Rotamer averaging was apparent for several residues (Table 3). Significant rotamer averaging in the E:folate complex was observed in residues Ile14 ($\chi^1 = \pm 60°$), Thr35 ($\chi^1 = +60°/180°$), Ile94 ($\chi^1 = \pm 60°$), Val119 ($\chi^1 = -60°/180°$), and Thr123 ($\chi^1 = -60°/180°$). In some cases, the heterogeneity was apparent from different crystal structures: for example, Val119 and Thr123 have χ^1 values that vary between crystal structures. The methyl groups in these residues, especially the Val119 γ1 and γ2 methyls, have low methyl S^2_{axis} (Figure 2) and large τ_e values, suggesting large amplitude motions within rotamer wells and possibly fast (picosecond/nanosecond time scale) jumping between wells. In contrast, values of S^2_{axis} for the methyls of Ile14, Thr35, and the Ile94-δ1 methyl are close to the methyl-type average, implying that the deuterium relaxation is dominated by restricted picosecond time scale motions within rotamer wells and implying that jumps between rotamer wells occur on a time scale slower than the rotational correlation time (ca. 10 ns).

In the ternary E:folate:NADP$^+$ complex, Val119 primarily populates the $\chi^1 = -60°$ rotamer (68%). At the same time, the methyl S^2_{axis} value for Val119-γ2 increases ($\Delta S^2 \sim 0.2$) (Figure 4b). A change in rotamer distribution is also reflected in the χ^1 rotamer populations of the strictly conserved residue Ile14. In the occluded loop conformation, the two gauche conformations of χ^1 in Ile14 are roughly equally probable; however, the population of the $\chi^1 = +60°$ rotamer increases significantly in the closed conformation of the E:folate:NADP$^+$ complex (68%), averaged with a significant population of the trans rotamer. Stabilization of a single rotamer in the E:folate:NADP$^+$ complex may be related to contacts made with the nicotinamide ring. In the closed E:folate:NADP$^+$ complex, the backbone carbonyl of Ile14 hydrogen bonds to the carboxamide of the nicotinamide ring, restricting rotation in ψ (*11*).

It is notable that many of the methyl-containing residues that exhibit rotamer disorder are located in the substrate and cofactor-binding sites and in the interface between the Met20

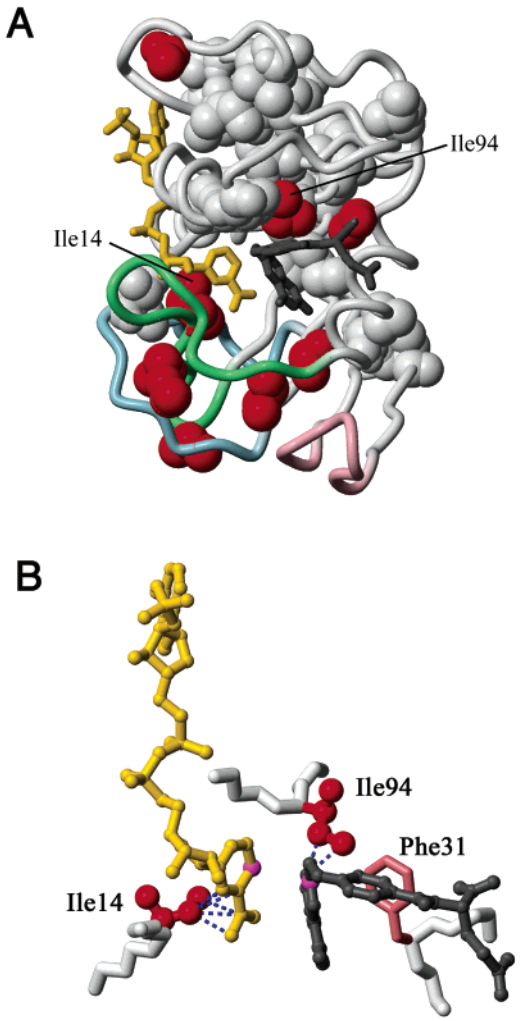

FIGURE 5: (a) View of the active site face of the DHFR ternary complex (1rx2) with folate and $NADP^+$ shown in black and gold, respectively. Isoleucine, threonine, and valine residues for which solution state χ^1 angles could be determined are represented as solid spheres equivalent in size to the van der Waals radii. Residues exhibiting a single χ^1 rotamer (>70% occupancy) are shaded white. Residues that exhibit χ^1 rotamer averaging are colored red. (b) A close-up view of the active site showing the side chains of Ile14 and Ile94 in the minor trans rotamer conformations; dotted lines indicate instances of steric clash between atoms of Ile14 and nicotinamide ring of the cofactor and between Ile94 and pterin ring of the substrate. The hydride donor and acceptor atoms of the cofactor and substrate are shown in magenta. The figures were generated using MOLMOL (*54*).

and the F-G loops (Figure 5a). In particular, the side chains of Ile14 and Ile94, which contact the nicotinamide and pterin rings, respectively, each populate both the gauche+ ($\chi^1 = +60°$) and trans ($\chi^1 = 180°$) rotameric states in the E:folate:$NADP^+$ complex; however, only the gauche+ rotamer is observed in the X-ray structures (*11*, *51*). In the minor trans rotamer (31% population) of Ile14, the γ1 methylene and δ1 methyl groups would undergo steric clash with the nicotinamide ring of the cofactor if it remained in its position in the X-ray structure (Figure 5b). The net effect would be an upward force on the nicotinamide, in the direction of the pterin ring of the substrate. Likewise, within the 1rx2 X-ray structure, the trans rotamer of Ile94 (46% population) also leads to unfavorable contacts with Phe31 and with the pterin ring of the bound folate; steric clash could be relieved by pushing the pterin ring toward the nicotinamide ring. Thus, the observation that the trans χ^1 rotamers of Ile14 and Ile94 are populated in solution implies the presence of significant conformational flexibility in the active site and suggests that the enzyme may sample states in which the nicotinamide and pterin rings are closer together than is observed in the static crystal structures. In the calculated optimal geometry of the transition state (*52*), the distance between the donor and the acceptor carbon atoms (nicotinamide C4 and pterin C6) involved in the hydride transfer is significantly closer than in the X-ray structures of the E:folate:$NADP^+$ complex (*11*). Thus, the trans χ^1 rotamers of Ile14 and Ile94 could play a role in transition state stabilization. Also, side chain fluctuations involving the trans rotameric state could direct the motion of the nicotinamide and pterin rings toward each other, thereby facilitating the hydride transfer. In support of this function, we note that recent quantum mechanical/classical molecular dynamics simulations suggest that Ile14 is part of a network of dynamically coupled residues that promote catalysis in DHFR, helping to direct the donor toward the acceptor through motions of its side chain (*45*). An Ile14Ala mutation has been shown to decrease the hydride transfer rate by nearly 20-fold (*53*).

Several methyl resonances were severely broadened in spectra of the E:folate:$NADP^+$ complex (data not shown), suggesting the presence of motions on the chemical shift time scale (i.e., on a time scale of microseconds to milliseconds). The broadened resonances are associated with residues in and around the active site (Ala7-β, Ile14-δ1, Ala19-β, and Ala117-β), indicating extensive slow time scale motions in the E:folate:$NADP^+$ complex. Broadening is unlikely to arise from substrate or $NADP^+$ exchange, which is much too slow to have a significant effect on line widths (*10*). The broadening observed for the δ1 methyl resonance of Ile14, a residue that undergoes χ^1 rotamer averaging, is of particular interest. This methyl group packs tightly against the nicotinamide ring: resonance broadening could result from motions in the Ile14 side chain itself (such as conformational transitions between the gauche+ and trans χ^1 rotamers discussed above) or from fluctuations in the nicotinamide ring, both of which could modulate the chemical shift on the microsecond/millisecond time scale.

CONCLUSION

Side chain motions in *E. coli* DHFR have been probed by measurement of methyl deuterium relaxation rates and side chain coupling constants. A motionally restricted hydrophobic core that encompasses part of the substrate-binding site is seen in both the E:folate and E:folate:$NADP^+$ complexes. However, significant changes are observed in methyl dynamics for residues in the active site loops and in the adenosine-binding site on transition to the closed E:folate:$NADP^+$ complex, which is considered to be an analogue of the Michaelis complex. Several methyl-containing side chains in the Met20 and F-G loops become more rigid. Loss of flexibility in the F−G loop and at the active site is confirmed by the absence of χ^1 rotamer averaging in the closed E:folate:$NADP^+$ complex. On the basis of comparisons with X-ray structures and theoretical calculations (*11*, *45*), rotamer averaging that does persist in the E:folate:$NADP^+$ complex may reflect motions that are along the catalytic pathway. Although some motions on the picosecond/nanosecond time scale are restricted, methyl resonances from several side

chains in the active site of the E:folate:$NADP^+$ ternary complex are severely broadened, suggesting the presence of new motions on the microsecond/millisecond time scale.

ACKNOWLEDGMENT

John Chung is gratefully acknowledged for assistance with implementing the deuterium relaxation experiments, and we thank Dr. Stephen Benkovic for invaluable discussions.

SUPPORTING INFORMATION AVAILABLE

Methyl ^2H R_1 and $R_{1\rho}$ relaxation rates measured at ^1H spectrometer frequencies of 600 and 800 MHz and the coupling constants $^3J_{C\gamma CO}$ and $^3J_{C\gamma N}$. This material is available free of charge via the Internet at http://pubs.acs.org.

REFERENCES

1. Bialek, W., and Onuchic, J. N. (1988) *Proc. Natl. Acad. Sci. U.S.A. 85*, 5908−5912.
2. Daizadeh, I., Medvedev, E. S., and Stuchebrukhov, A. A. (1997) *Proc. Natl. Acad. Sci. U.S.A. 94*, 3703−3708.
3. Arnesano, F., Banci, L., Bertini, I., Felli, I. C., and Koulougliotis, D. (1999) *Eur. J. Biochem. 260*, 347−354.
4. Kohen, A., Jonsson, T., and Klinman, J. P. (1997) *Biochemistry 36*, 2603−2611.
5. Kohen, A., Cannio, R., Bartolucci, S., and Klinman, J. P. (1999) *Nature 399*, 496−499.
6. Brooks, C. L., III, Karplus, M., and Pettitt, B. M. (1988) A theoretical perspective of dynamics, structure, and thermodynamics *Adv. Chem. Phys., 71*, 1−259.
7. Warshel, A. (2002) *Acc. Chem. Res. 35*, 385−395.
8. Vihinen, M. (1987) *Protein Eng 1*, 477−480.
9. Zavodszky, P., Kardos, J., Svingor, and Petsko, G. A. (1998) *Proc. Natl. Acad. Sci. U.S.A. 95*, 7406−7411.
10. Fierke, C. A., Johnson, K. A., and Benkovic, S. J. (1987) *Biochemistry 26*, 4085−4092.
11. Sawaya, M. R., and Kraut, J. (1997) *Biochemistry 36*, 586−603.
12. Miller, G. P., and Benkovic, S. J. (1998) *Biochemistry 37*, 6336−6342.
13. Miller, G. P., Wahnon, D. C., and Benkovic, S. J. (2001) *Biochemistry 40*, 867−875.
14. Osborne, M. J., Schnell, J., Benkovic, S. J., Dyson, H. J., and Wright, P. E. (2001) *Biochemistry 40*, 9846−9859.
15. Mittermaier, A., Kay, L. E., and Forman-Kay, J. D. (1999) *J. Biomol. NMR 13*, 181−185.
16. Wand, A. J., Urbauer, J. L., McEvoy, R. P., and Bieber, R. J. (1996) *Biochemistry 35*, 6116−6125.
17. Muhandiram, D. R., Yamazaki, T., Sykes, B. D., and Kay, L. E. (1995) *J. Am. Chem. Soc. 117*, 11536−11544.
18. Yang, D. W., Mittermaier, A., Mok, Y. K., and Kay, L. E. (1998) *J. Mol. Biol. 276*, 939−954.
19. Yang, D., and Kay, L. E. (1996) *J. Magn. Reson., Ser. B 110*, 213−218.
20. Epstein, D. M., Benkovic, S. J., and Wright, P. E. (1995) *Biochemistry 34*, 11037−11048.
21. Miller, G. P., and Benkovic, S. J. (1998) *Biochemistry 37*, 6327−6335.
22. Kay, L. E., Ikura, M., and Bax, A. (1990) *J. Am. Chem. Soc. 112*, 888−889.
23. Montelione, G. T., Lyons, B. A., Emerson, S. D., and Tashiro, M. (1992) *J. Am. Chem. Soc. 114*, 10974−10975.
24. Osborne, M. J., Venkitakrishnan, R. P., Dyson, H. J., and Wright, P. E. (2003) *Protein Sci. 12*, 2230−2238.
25. Falzone, C. J., Benkovic, S. J., and Wright, P. E. (1990) *Biochemistry 29*, 9667−9677.
26. Falzone, C. J., Cavanagh, J., Cowart, M., Palmer, A. G., Matthews, C. R., Benkovic, S. J., and Wright, P. E. (1994) *J. Biomol. NMR 4*, 349−366.
27. Rosen, M. K., Gardner, K. H., Willis, R. C., Parris, W. E., Pawson, T., and Kay, L. E. (1996) *J. Mol. Biol. 263*, 627−636.
28. Neri, D., Szyperski, T., Otting, G., Senn, H., and Wüthrich, K. (1989) *Biochemistry 28*, 7510−7516.
29. Viles, J. H., Duggan, B. M., Zaborowski, E., Schwarzinger, S., Huntley, J. J., Kroon, G. J., Dyson, H. J., and Wright, P. E. (2001) *J. Biomol. NMR 21*, 1−9.
30. Palmer, A. G., Rance, M., and Wright, P. E. (1991) *J. Am. Chem. Soc. 113*, 4371−4380.
31. Press, W. H., Teukolsky, S. A., Vetterling, W. T., and Flannery, B. P. (1992) *Numerical Recipes in C*, Cambridge University Press, Cambridge, UK.
32. Lipari, G., and Szabo, A. (1982) *J. Am. Chem. Soc. 104*, 4546−4559.
33. Lipari, G., and Szabo, A. (1982) *J. Am. Chem. Soc. 104*, 4559−4570.
34. Osborne, M. J., and Wright, P. E. (2001) *J. Biomol. NMR 19*, 209−230.
35. Abragam, A. (1961) *Principles of Nuclear Magnetism*, Clarendon Press, Oxford.
36. Mittermaier, A., and Kay, L. E. (1999) *J. Am. Chem. Soc. 121*, 10608−10613.
37. Grzesiek, S., Vuister, G. W., and Bax, A. (1993) *J. Biomol. NMR 3*, 487−493.
38. Vuister, G. W., Wang, A. C., and Bax, A. (1993) *J. Am. Chem. Soc. 115*, 5334−5335.
39. Pachler, K. G. R. (1963) *Spectrochim. Acta 19*, 2085−2092.
40. Pachler, K. G. R. (1964) *Spectrochim. Acta 20*, 581−587.
41. Hennig, M., Bermel, W., Spencer, A., Dobson, C. M., Smith, L. J., and Schwalbe, H. (1999) *J. Mol. Biol. 288*, 705−723.
42. Perez, C., Lohr, F., Ruterjans, H., and Schmidt, J. M. (2001) *J. Am. Chem. Soc. 123*, 7081−7093.
43. Falzone, C. J., Wright, P. E., and Benkovic, S. J. (1994) *Biochemistry 33*, 439−442.
44. Rajagopalan, P. T., Lutz, S., and Benkovic, S. J. (2002) *Biochemistry 41*, 12618−12628.
45. Agarwal, P. K., Billeter, S. R., Rajagopalan, P. T. R., Benkovic, S. J., and Hammes-Schiffer, S. (2002) *Proc. Natl. Acad. Sci. U.S.A. 99*, 2794−2799.
46. Bax, A., Vuister, G. W., Grzesiek, S., Delaglio, F., Wang, A. C., Tschudin, R., and Zhu, G. (1994) *Methods Enzymol. 239*, 79−105.
47. Chou, J. J., Case, D. A., and Bax, A. (2003) *J. Am. Chem. Soc. 125*, 8959−8966.
48. Skrynnikov, N. R., Millet, O., and Kay, L. E. (2002) *J. Am. Chem. Soc. 124*, 6449−6460.
49. Goodman, J. L., Pagel, M. D., and Stone, M. J. (2000) *J. Mol. Biol. 295*, 963−978.
50. Reyes, V. M., Sawaya, M. R., Brown, K. A., and Kraut, J. (1995) *Biochemistry 34*, 2710−2723.
51. Bystroff, C., Oatley, S. J., and Kraut, J. (1990) *Biochemistry 29*, 3263−3277.
52. Wu, Y., and Houk, K. N. (1987) *J. Am. Chem. Soc. 109*, 906−908.
53. Adams, J. A., Fierke, C. A., and Benkovic, S. J. (1991) *Biochemistry 30*, 11046−11054.
54. Koradi, R., Billeter, M., and Wüthrich, K. (1996) *J. Mol. Graphics 14*, 51−55.

BI035464Z